ELECTROCHEMICAL INVESTIGATION ON 1,2,3,4-TETRAHYDROACRIDINE-9-CARBOXAMIDE IN DIFFERENT ORGANIC SOLVENTS

Madalina Marina HRUBARU[1,2], Francis Aurelien NGOUNOUE KAMGA[3], Nathanael MURAT[4], Constantin DRAGHICI[1], Magdalena-Rodica BUJDUVEANU[4], Eleonora-Mihaela UNGUREANU[2*], Elena DIACU[2]

The electrochemical investigations of 1,2,3,4-tetrahydroacridine-9-carboxamide (MM1) were carried out in two organic solvents, acetonitrile (ACN) and dimethylformamide (DMF), using three methods: cyclic voltammetry, differential pulse voltammetry, and rotating disk electrode voltammetry, following standard procedures. The values of the principal peak potentials were recorded in millimolar solutions of MM1 in ACN and DMF solvents in presence of 0.1 M tetrabutylammonium perchlorate. The behavior of MM1 in ACN is similar to that in DMF in the cathodic domains. In the anodic domains, two oxidation peaks are observed only in ACN, and no oxidation peak in DMF. Main differences appear in the anodic domains, where two anodic irreversible processes appear only in ACN. The diffusion coefficients for MM1, calculated using Randles-Sevcik equation, are $4.61 \cdot 10^{-5}$ cm^2/s for ACN, and $0.82 \cdot 10^{-5}$ cm^2/s.in DMF. These electrochemical studies provide the basis for understanding the electrochemical properties of other tetrahydroacridines.

Keywords: 1,2,3,4-tetrahydroacridine-9-carboxamide, cyclic voltammetry, differential pulse voltammetry, rotating disk electrode voltammetry, diffusion coefficients

1. Introduction

Nowadays π-conjugated organic molecules have become substances with a great impact on several cutting-edge fields such as organic electronics, ion detection and solar cell development [1-4]. For example, acridines are π-conjugated heteroaromatic compounds [5] well known especially for their numerous applications in different branches of medicinal chemistry [6], dye industry [7] and

[1] "C. D. Nenitzescu" Institute of Organic and Supramolecular Chemistry", Romanian Academy, Romania, Bucharest, e-mail: madalina_marina@yahoo.com
[2] Doctoral School - Chemical Engineering and Biotechnologies, National University of Science and Technology POLITEHNICA Bucharest, Romania, e-mail: em_ungureanu2000@yahoo.com
[3] Coordination Chemistry Laboratory, Department of Inorganic Chemistry, Faculty of Science, University of Yaounde 1, Yaounde P.O. Box 812, Cameroon, e-mail: fr.kamga@gmail.com
[4] Faculty of Chemical Engineering and Biotechnologies, National University of Science and Technology POLITEHNICA Bucharest, Romania, e-mail: murat_nathanael@yahoo.com

metal chemosensing [8]. Having a strong electron donating capacity [9] and interesting optoelectronic properties [10], acridines are also attractive for the field of organic light-emitting diodes [11]. Despite the fact that increasing attention has been given to the photophysical features of acridines, their analogues-tetrahydroacridines – which are partially hydrogenated have not received the same attention, although they have been used as electron-donating compounds for OLED applications [12]. The use of some tetrahydroacridines in pharmaceutical chemistry is due to their capacity to inhibit topoisomerase enzymes, to block DNA transcription [13], [14], human cancer [15], and tuberculosis [16].

Considering the huge potential of tetrahydroacridines in the field of pharmaceutical chemistry as well as the lack of knowledge regarding their optoelectronic properties, the search for new candidates is of continuous interest. The synthesis of bis-tetrahydroacridines derived from benzidine and p,p'-diphenylmethane has recently received a special attention in our laboratory [17]. This is a continuation of our work and part of our previous interest in new organic materials [18] electrochemical investigation. In order to understand tetrahydroacridines' electrochemical behavior several compounds of this class were investigated experimentally. In this paper are presented the results of electrochemical studies for 1,2,3,4-tetrahydroacridine-9-carboxamide (MM1) with the chemical structure given in Fig.1.

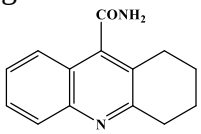

Fig. 1. Chemical structure of 1,2,3,4-tetrahydroacridine-9-carboxamide (MM1)

MM1 tetrahydroacridine derivative was synthesized according to a previously described method [19], and its physical chemical characteristics were established to confirm the structure. We have reported recently its optical behavior, and the results of DFT calculations [20]. The present paper enlarges the properties of interest for this compound with the results obtained by electrochemistry studies.

2. Experimental

Synthesis of investigated compound was performed according to a previously described methods [19]. Acetonitrile (ACN) (Sigma Aldrich, 99.999%), dimethylformamide (DMF), and tetrabutylammonium perchlorate (TBAP) from Fluka were used as received. All *electrochemical measurements* were performed using an Autolab 302N potentiostat connected to a three-electrode cell. The working electrode used for the electrochemical characterization was a glassy carbon (GC) disk with a diameter of 3 mm (Metrohm). A platinum wire was used as the counter electrode. Ag/10 mM $AgNO_3$, 0.1 M TBAP in acetonitrile (CH_3CN) solution was used as reference electrode. All potentials were reported at the end of

the experiments to the potential of the ferrocene/ferrocenium (Fc/Fc^+) redox couple in 0.1 M TBAP, CH_3CN. The electrochemical investigations carried out for the electrochemical characterization of the compound consisted of three electrochemical methods, namely cyclic voltammetry (CV), differential pulse voltammetry (DPV) and rotating disk electrode voltammetry (RDE), applying similar methods [18]. Before each determination, the surface of the GC working electrode was polished with diamond paste, then wiped with fine paper.

3. Results

The electrochemical investigations of MM1 tetrahydroacridine derivative were accomplished in its millimolar solutions in ACN and DMF, using the same electrolyte TBAP in the same concentration (0.1 M). The curves were recorded in the potential ranges between −3.5 V and +3 V. The potential axis was referred to the ferrocene/ferrocenium (Fc/Fc^+) redox couple potential after the experiments in order to allow the future comparison of many tetrahydroacridines. Each scan was started from the equilibrium potential to an anodic or cathodic limit, according to the processes to be investigated. Potential starting points and scan direction are shown by arrows on the curves presented in this paper.

3.1 DPV, CV, and RDE experiments

The DPV, CV, and RDE curves for MM1 obtained in the two solvents are shown in parallel in Fig. 2-8 for experiments performed in acetonitrile (a) and DMF (b). Anodic (a) and cathodic (c) peaks were denoted on the curves taking into account the peaks on the DPV curves, where the processes were better evidenced. The 3 electrochemical methods used gave different results, which were correlated, according to each procedure characteristics. That is why the CV and RDE curves were sometimes presented under the DPV curves. For instance, in Figure 8 the CV curves (b) and RDE curves (c) at different concentrations of MM1 in the two solvents are shown under and the corresponding DPV curves, having the same potential scales. The values of the principal peak potentials from MM1 CV and DPV curves recorded in MM1 solutions (1mM) in ACN and DMF solvents in presence of TBAP (0.1 M) are given in Table 1:

Table 1

Values for the main peak potentials (*vs.* Fc/ Fc^+) from CV and DPV curves of MM1 in ACN and DMF solvents in presence of 0.1 M TBAP ([MM1] = 1 mM).

Solvent	ACN		DMF	
Peak\ Parameter	E_{CV}(V)	E_{DPV}(V)	E_{CV}(V)	E_{DPV}(V)
a1	1.501	1.468	-	-
a2	2.165	2.037	-	-
c1	-2.279	-2.241	-2.460	-2.392
c2	-2.518	-2.422	-2.622	-2.593

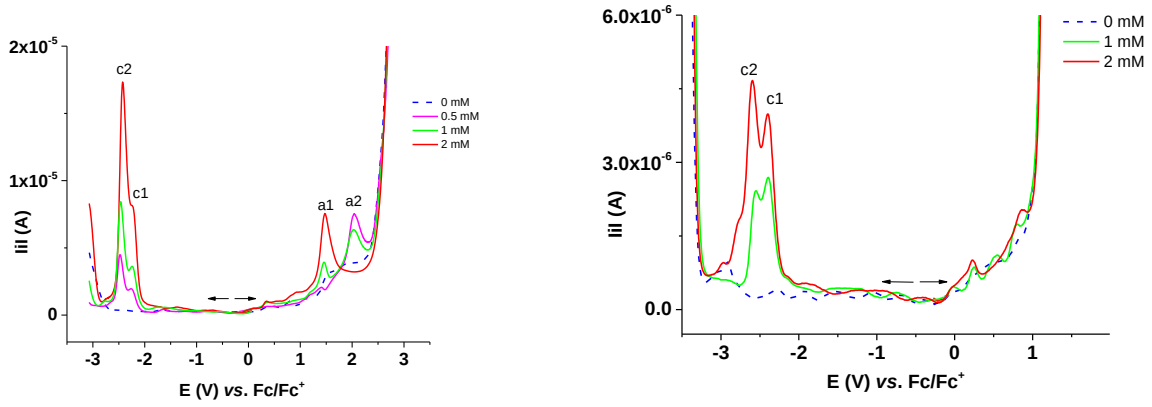

a b

Fig. 2. Anodic and cathodic DPV curves for MM1 solutions in ACN (a) and DMF (b) at different concentrations.

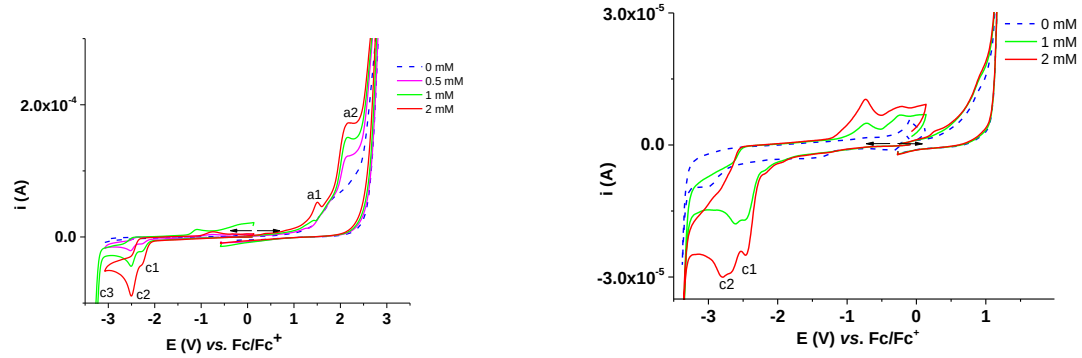

a b

Fig. 3. Anodic and cathodic CV curves for MM1 solutions in ACN (a) and DMF (b) at different concentrations.

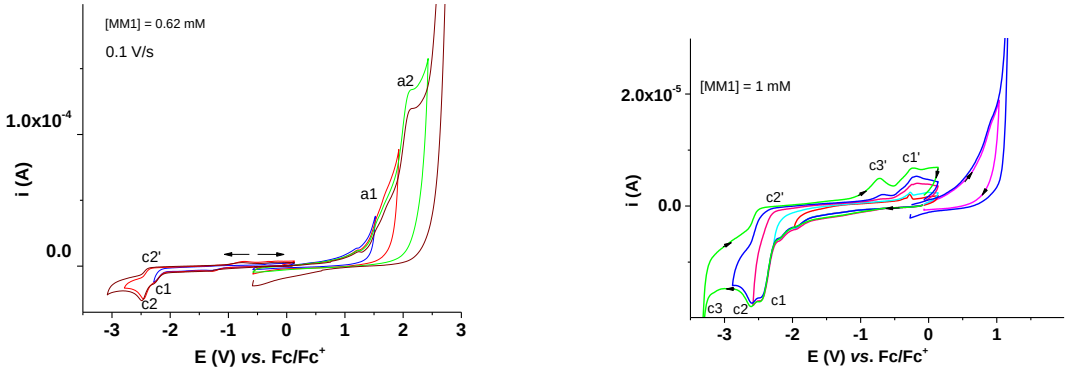

a b

Fig. 4. Anodic and cathodic CV curves for MM1 solutions in ACN (a) and DMF (b) over different potential domains.

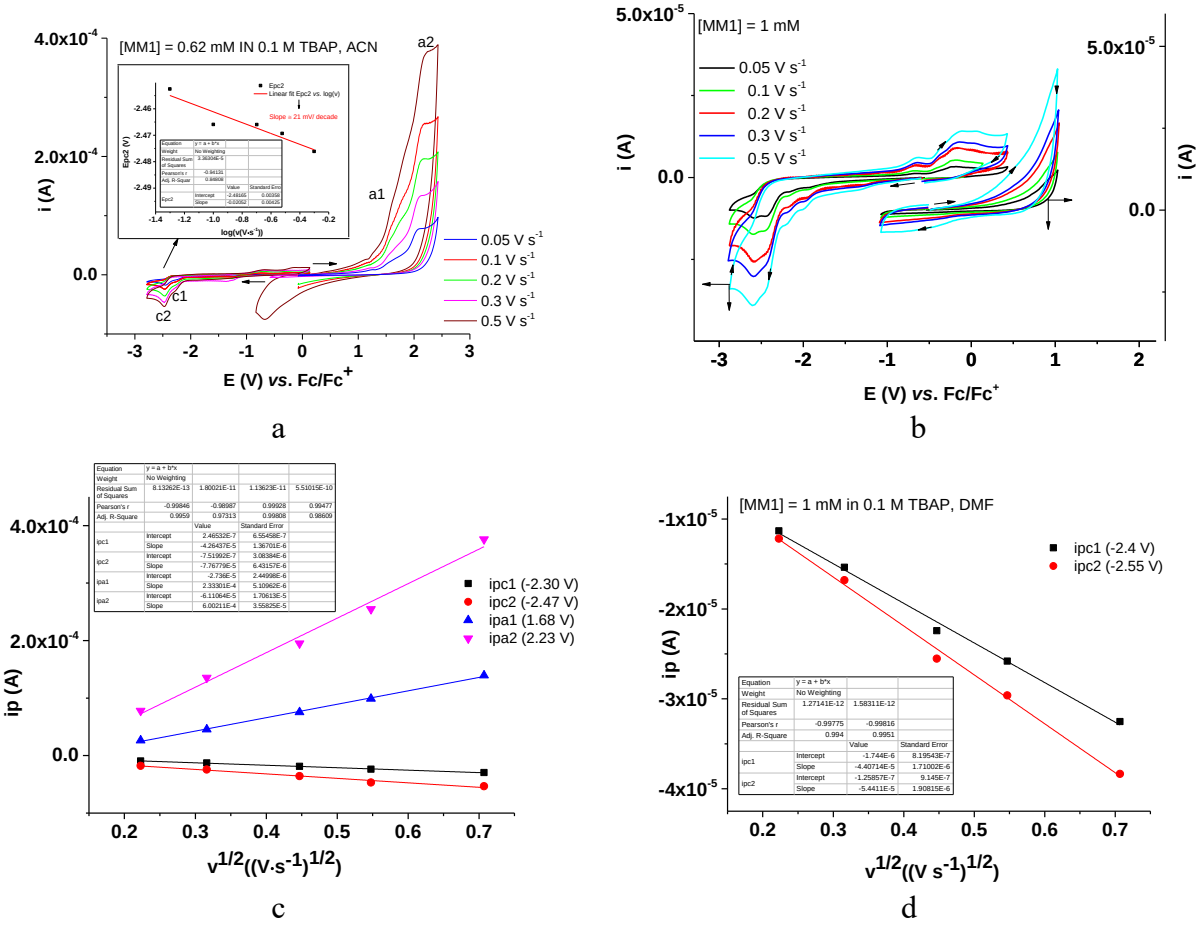

Fig. 5. Anodic and cathodic CV curves for MM1 solutions in ACN (a) and DMF (b) at different potential scan rates and the dependencies of cathodic peak currents on the square root of the scan rate in ACN (c) and DMF (d); (a) inset: Linear dependence of c2 peak potential on the logarithm of the scan rate from Fig. 5a.

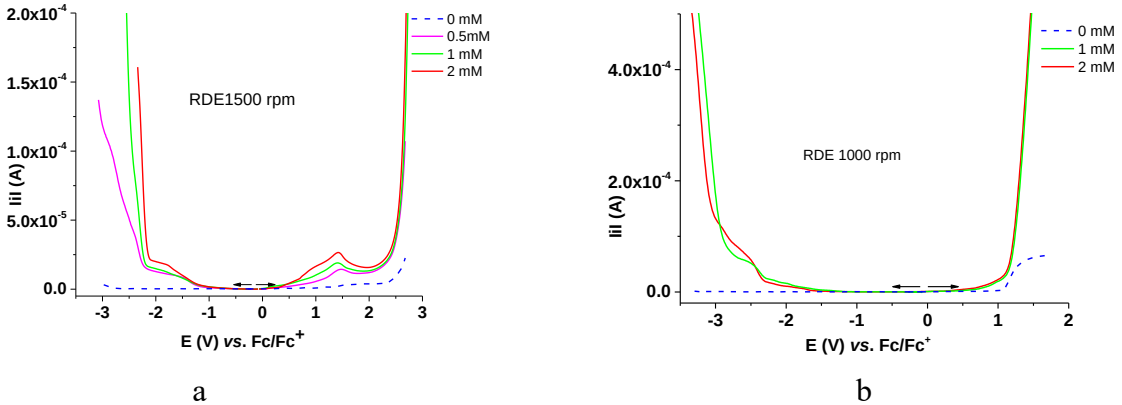

Fig. 6. Anodic and cathodic RDE curves for MM1 solutions in ACN (a) and DMF (b).

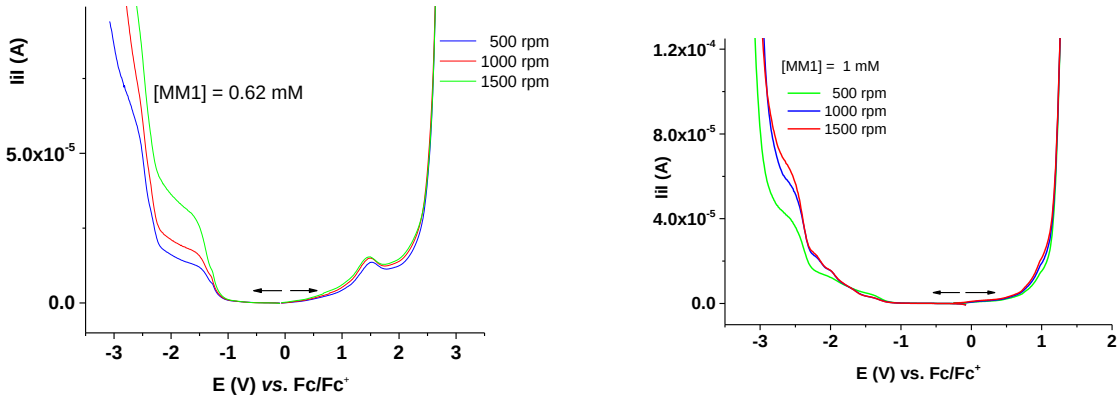

Fig. 7. Anodic and cathodic RDE curves at different rotations rates in MM1 solutions in 0.1 M TBAP in ACN (a) and DMF (b).

3.2 Comparison between DPV, CV and RDE voltammetric curves for MM1 in ACN and in DMF

Examination of the DPV curves in both solvents (Fig. 2) indicates that MM1 presents in ACN in the cathodic region two closed peaks situated at -2.241 V (c1) and -2.422 V (c2), while in DMF they appear more distant (Table 1). That is why in ACN the intensity of c1 appears about 2 times higher than c2. The potential shift between c1 and c2 is 0.18 V in ACN and 0.2 V in DMF. In the anodic region two peaks are visible only in ACN, and not in DMF. The cathodic currents for peaks c1 and c2 and the anodic current for peak a1 increase with the concentration of MM1, while the anodic current for a2 decreases with the concentration. The last feature is connected with the background interference. The anodic processes for MM1 are located at potentials at which the oxidation processes of the supporting electrolyte also occur, so the currents are sums of the processes occurring at each potential.

Fig. 3 shows the CV curves for MM1 in both solvents for different concentrations. The potentials obtained in the CV curves are in agreement with those obtained by DPV. Also, it can be seen that the oxidation process of the supporting electrolyte in the CV is important and it masks the oxidation processes of MM1 at concentrations lower than 2 mM for peak a1. In DMF, the cathodic processes c1 and c2 for MM1 are clearly differentiated compared to the solvent, in which evolution occurs at the peak potential denoted by c3 in Fig. 3. Instead, the anodic processes of the solvent completely mask the anodic oxidation peaks.

Fig. 4 shows anodic and cathodic CV curves on different potential domains and highlights quasi-reversible c1 and c2 cathodic processes and irreversible anodic processes in both solvents. Cathodic processes are much better highlighted in DMF and anodic processes are seen as peaks only in ACN.

The anodic and cathodic CV curves for MM1 solutions in ACN (a) and DMF (b) from Fig. 5 shows the increase of the peak currents with the scan rate. The dependencies of cathodic peak currents on the square root of the scan rate in ACN (c) and DMF (d) are linear (Fig, 5 c and d). The equation slopes are given in Table 2.

The RDE anodic and cathodic curves for MM1 in solutions in ACN (a) and DMF (b) shown in Fig.6 indicated very clear increase of the cathodic peak currents and small increase of the anodic peak current in ACN when the concentration of MM1 increases. In DMF there is a small increase of the cathodic peak currents and no increase of the anodic current when the concentration of MM1 increases.

Cathodic RDE curves at different rotations rates shown in Fig.7 indicate higher regular increase of limiting currents for processes in ACN (Fig, 7a) than in DMF (Fig, 7b). Anodic RDE curves at different rotations rates from Fig.7a have the form of *peak* instead of a *wave*, with a small increase of the currents in ACN, suggesting the covering of the electrode with insulating products at anodic potentials. Their formation is confirmed by the recording of successive CV curves, in which the currents drop in successive cycles (Fig. 9 and Fig. 10) and the peak potential is shifted toward positive potentials when cycling (Fig. 9). There is no increase in DMF with the rotation rate for anodic currents (Fig. 7b).

Fig. 8 underlines the differences between the curves recorded by CV (a), DPV (b), and RDE (c) methods in ACN (red colored curves) and DMF (blue colored curves) for MM1 (continuous lines) and backgrounds (dashed lines). The last ones resulted from electrochemical processes of TBAP in ACN (dashed red colored curves) and DMF (dashed blue colored curves) used as supporting electrolytes.

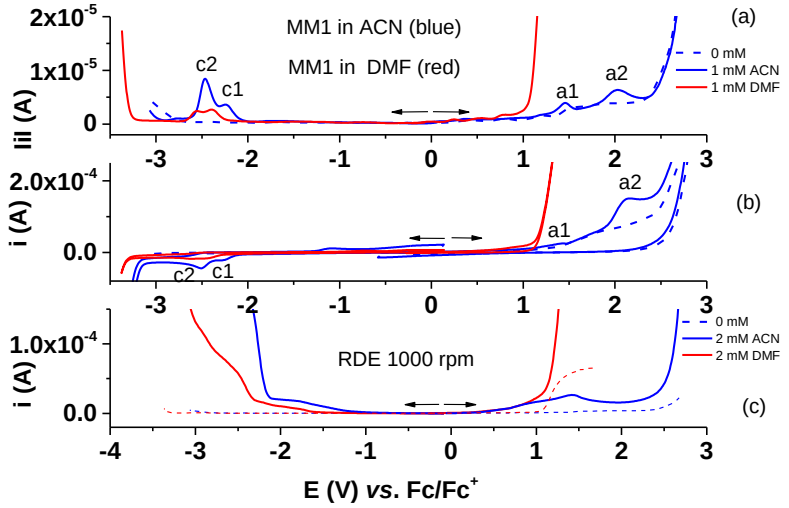

Fig. 8. DPV(a), CV (b), and RDE (c) anodic and cathodic curves for [MM1] = 1 mM (a, b) and [MM1] = 2 mM (c) in ACN (blue lines) and DMF (red lines).

The peak currents for oxidation and reduction of MM1 increase linearly with the concentration of MM1 and with the square root of the scan rate in CV experiments. The equations of the linear dependences of the main CV peak currents on the scan rate in ACN and DMF solvents in [MM1] = 1 mM in presence of 0.1 M TBAP are given in Table 2.

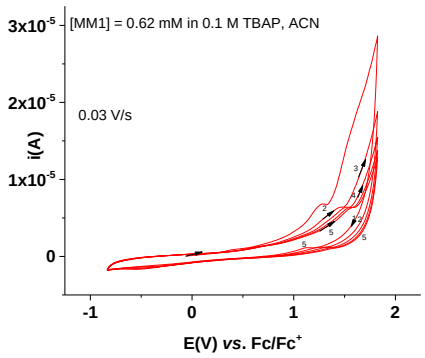

Fig. 9. Successive CV cycles (5) in the domain of a1 peak (0.03 V/s) in [MM1] = 0.62 mM in ACN

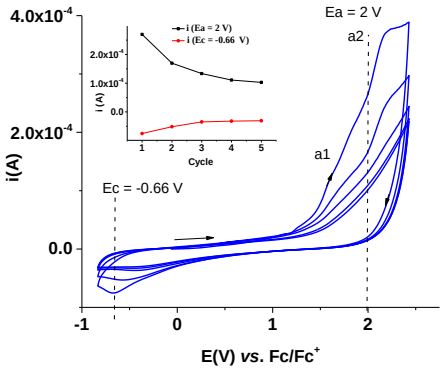

Fig. 10. Successive CV (0.5 V/s) cycles (5) in [MM1] = 0.62 mM in the domain of a2 peak in ACN; inset: anodic and cathodic currents vs. number of cycles.

3.3. Mechanism schemes for electrochemical processes

The proposed mechanisms for the electrochemical processes occurring during the potential scans are in accordance with the observations made through the

study by DPV, CV and RDE. They are similar with other mechanistic schemes developed for other compounds with acridine-related structure [21]. The electrochemical oxidation mechanism of MM1 is shown in Scheme 1. Scheme 2 shows the resonance structures for the intermediate cation radical formed during the oxidation of MM1. The electrochemical reduction mechanism of MM1 is shown in Scheme 3.

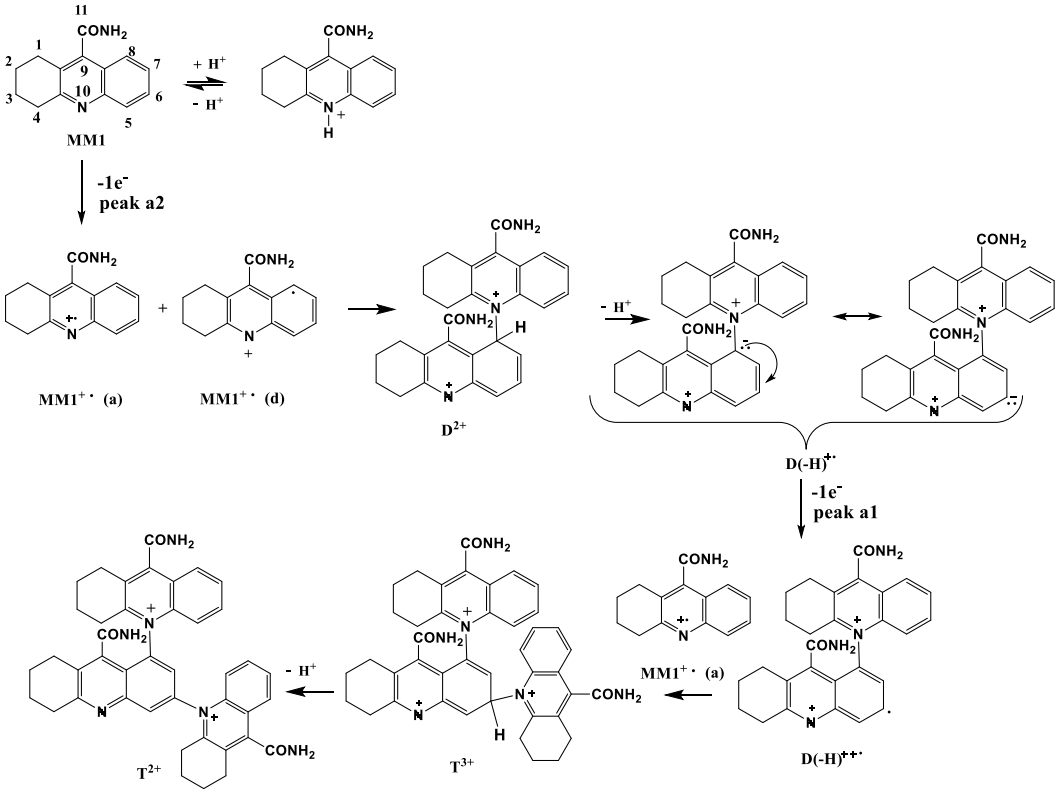

Scheme 1. Electrooxidation mechanism of MM1.

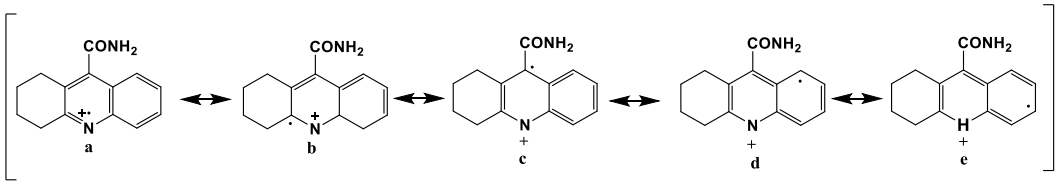

Scheme 2. Resonance structures for the intermediate radical cation formed during the oxidation of MM1.

The oxidation process involves globally two electrons and two protons (Scheme 1), with the formation of a intermediate dimer dication radical (D^{2+}). A monomer radical cation ($MM1^{+\bullet}$) is formed in the first step after the irreversible electron transfer. It has five resonance structures (a-e in Scheme 2). Due to the

unpaired electron which is delocalized in $MM1^{+\bullet}$ radical cation, the attack site of the MM1 radical cation for dimerization may be at positions 8 or 6, while positions 5a and 9 are less likely due to the steric hindrance (see second line in Scheme 1). Consequently, it can be assumed that two radical cation monomers of MM1 would dimerize (by forming a C-N bond in D^{2+}) which deprotonates to $D(-H)^{+\bullet}$, and then proceed to the second consecutive electron transfer, leading to $D(-H)^{++\bullet}$ radical dication, as shown in the third line of Scheme 1. The process can continue with the formation of a polymer, like indicated in the third line of Scheme 1. Therefore, high molecular mass products could be accumulated on the electrode surface by electron transfers and chemical (radical couplings, deprotonations) successive steps.

Scheme 3 shows the two-stage electrochemical reduction mechanism of MM1. A two-stage electrochemical reduction was proposed taking into account the curves obtained during the reduction processes of MM1. It involves the formation of $MM1(H)^{\bullet}$ in the first step, and of 1,2,3,4,4a,10-hexahydroacridine-9-carboxamide ($MM1H_2$) in the second step as a final product of C=N double bond electrochemical reduction.

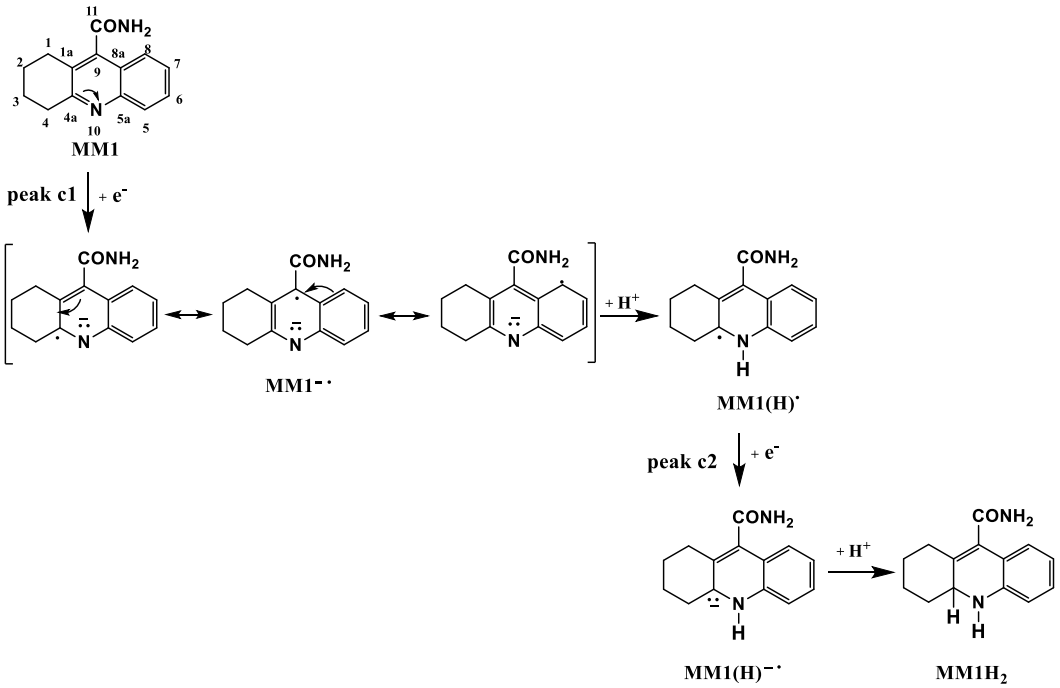

Scheme 3. The two-stage electrochemical reduction mechanism of MM1.

3.4. Diffusion coefficients for MM1 in ACN and DMF

The fact that the absolute value of peak currents for MM1 increased linearly with the square root of the scan rate (Fig. 5) indicates these processes are diffusion

controlled. This was confirmed by the linear dependence of Ep *vs* logv, with slope values of 21 mV/ decade (Fig. 5a inset). Some adsorption of the electroactive material also took place, as indicated by the small intercept in the above-mentioned equations, ip *vs*. $v^{1/2}$, in addition to diffusion of electroactive material. According to Fig. 10, the oxidation currents (at Ea = 2 V) and their corresponding currents in reduction (Ec = -0.66 V) in absolute value decreased from the first to the second and continuously to the fifth cycle (Fig. 10 inset). This phenomenon may have been attributed to consumption of the adsorbed MM1 product or presence of an electropolymerization product on the electrode surface.

The dependence of the cathodic and anodic currents on the square root of the scan rate from Fig. 5 (a and b) allowed the estimation of the diffusion coefficients of MM1 in the two solvents (Table 3), with the help of Randles-Sevcik equation (1) for the CV voltametric peaks. In equation (1) ip is the peak current in ampere, n represents the number of electrons transferred during the electrochemical step, A is the electrode surface area in cm^2, D is the diffusion coefficient in $cm^2 \cdot s^{-1}$, C is MM1 concentration in $mol \cdot cm^{-3}$ and v is scan rate in V/s. The value of the electrochemically active surface area of the working electrode was the geometrical area of the disk, A = 0.07065 cm^2.

$$ip = 2.68 \cdot 10^5 \cdot n^{3/2} \cdot A \cdot C \cdot D^{1/2} \cdot v^{1/2} \quad (1)$$

From the slopes of the linear dependences ip *vs*. $v^{1/2}$ given by $2.68 \cdot 10^5 \cdot n^{3/2} \cdot A \cdot C \cdot D^{1/2}$ for different peaks, D values were calculated in both solvents (D_{ACN} and D_{DMF}) at the potential of each peak Ep.

The diffusion coefficients were calculated in ACN and DMF (Table 3) using the dependencies of the reduction currents for peak c1 or c2, as well as the dependencies of the oxidation current for peak a1. In the case of reduction, the two peaks c1 and c2 are attributed exclusively to MM1 because the solvent processes are reduced in intensity both in ACN and in DMF. In case of MM1 oxidation, the curves show peak currents only in ACN. Of the two peaks a1 and a2 (noticed in ACN), only the peak a1 can be taken into account for the calculation of the diffusion coefficient; a2 peak cannot be used for this calculation because at this potential the oxidation processes of the solvent are important in terms of intensity and interference.

In equation (1) for the peaks c1, c2 and a1 were considered both cases: n=1 and n=2, for reasons related to the mechanism proposed for the reduction. The corresponding values for D are shown in Table 3. In ACN, the diffusion coefficient can be calculated both from the variations of the peak currents for c1 and c2 and from the variation of the peak current for the anodic process a1. The calculations performed and shown in Table 3 show close values for the diffusion coefficient of MM1 in ACN (D_{ACN}) only for the cathodic process c2 with n = 1, and the anodic process a1 with n = 2 (bold values on 6^{th} column of Table 3).

Table 2

Equations of the fitted lines of the main DPV peak currents ip (A) *vs.* the square root of the scan rate (v in V/s) in ACN and DMF solvents in [MM1] = 1 mM in presence of 0.1 M TBAP.

Solvent	Peak\ Parameter	ip *vs.* $v^{1/2}$	Pearson's R
DMF	a1	ipa1(0.9 V) = $-2.348 \cdot 10^{-6}+4.617 \cdot 10^{-5}\cdot v^{1/2}$	0.9925
	a2	-	
	c1	ipc1(-2.392 V) = $-1.744 \cdot 10^{-6}-4.407 \cdot 10^{-5}\cdot v^{1/2}$	-0.9978
	c2	ipc2(-2.553 V) = $-1.\ 259 \cdot 10^{-7}-5.441 \cdot 10^{-5}\cdot v^{1/2}$	-0.9982
ACN	a1	ipa1(1.680 V) = $-2.736 \cdot 10^{-5}+2.333 \cdot 10^{-4}\cdot v^{1/2}$	0.9993
	a2	ipa2(2.037 V) = $-6.111 \cdot 10^{-5}+6.002 \cdot 10^{-4}\cdot v^{1/2}$	0.9948
	c1	ipc1(-2.241 V) = $2.465 \cdot 10^{-7}-4.264 \cdot 10^{-5}\cdot v^{1/2}$	-0.9985
	c2	ipc2(-2.422 V) = $-7.520 \cdot 10^{-7}-7.768 \cdot 10^{-5}\cdot v^{1/2}$	-0.9899

Table 3

Diffusion coefficients calculation using the slopes (in A / $(V/s)^{1/2}$) of the fitted lines of the main CV peak currents in ACN ([MM1] = 0.62 mM) and DMF ([MM1] = 1 mM)

Crt. Nr.	Reference peak	n	E (V)	Slope	$10^5 \cdot D_{ACN}$ (cm^2/s)	Crt. Nr.	E (V)	Slope	$10^5 \cdot D_{DMF}$ (cm^2/s)
1	c1	1	-2.30	4.264E-5	1.31	7	-2.40	4.410E-5	0.53
2	c1	2	-2.30	4.264E-5	0.16	8	-2.40	4.410E-5	0.07
3	c2	1	-2.47	7.768E-5	**4.33**	9	-2.55	5.440E-5	**0.82**
4	c2	2	-2.47	7.768E-5	0.54	10	-2.55	5.440E-5	0.10
5	a1	1	1.680	2.333E-4	39.10	11	-	-	-
6	a1	2	1.680	2.333E-4	**4.89**	12	-	-	-

A mean value was kept for $D_{ACN} = 4.61 \cdot 10^{-5}$ cm^2/s. In this way, it was considered that the reduction of MM1 takes place in a diffusion-controlled process in two distinct single-electron steps, and the oxidation takes place in a1 in a two-electron process. Taking into account that the cathodic electrochemical processes of MM1 proceed similarly in ACN and DMF, which are very likely, because the CV, DPV, and RDE curves obtained are similar in these two organic solvents, the value of the diffusion coefficient in DMF for MM1 which corresponds to c2 peak with n =1 was considered (bold value). It resulted $D_{ACN} = 0.82 \cdot 10^{-5}$ cm^2/s.

The diffusion coefficient for MM1 in ACN is 5 times higher than in DMF, a fact which favorizes the electrochemical processes in ACN for this compound. Considering that the literature data from experiments performed with organic compounds in different electrolytes [22], these values for the diffusion coefficients in aprotic solvents are quite similar with other diffusion coefficients, and they vary similarly with the solvent being higher in ACN than in DMF. For instance, 1,4-anthraquinone with a molar mass of 208.22 (close to that of MM1 which is 226.11) has $D_{ACN} = 2.17 \cdot 10^{-5}$ cm^2/s, and $D_{DMF} = 1.01 \cdot 10^{-5}$ cm^2/s [22]. The results of electrochemical studies on MM1 enlarge the known properties of this compound and provide the basis for understanding the electrochemical properties of other important derivatives.

4. Conclusion

The electrochemical investigation of 1.2.3.4-tetrahydroacridine-9-carboxamide (MM1) was carried out in two organic solvents. acetonitrile (ACN) and dimethylformamide (DMF) in presence of 0.1 M tetrabutylammonium perchlorate put in evidence the reduction and oxidation peaks due to the electrochemical processes occurring during the potential scans. The values of potential and current for the main peaks were obtained using cyclic voltammetry and differential pulse voltammetry, as well as their variations with concentration and scan rate. Rotating disk electrode voltammetry underlined the characteristics of confirmed processes. The differences observed between the curves recorded by the same electrochemical method in the two solvents were examined and mechanisms of electrochemical reduction and oxidation were proposed to explain the processes seen on the experimental curves. The behavior of MM1 in ACN is similar to that in DMF in the cathodic domains. In the anodic domains two oxidation peaks are noticed in ACN, and no oxidation peak in DMF. The differences noted for the processes which occur in the anodic regions are due to the narrower potential limit of DMF compared to ACN. Therefore. the study of MM1 oxidation processes is only possible in ACN. because the potential window of this solvent is wider. The diffusion coefficients for MM1 are calculated using Randles-Sevcik equation. are favorable for ACN compared to DMF. being $4{,}61.82 \cdot 10^{-5}$ cm^2/s and $0.82 \cdot 10^{-5}$ cm^2/s, respectively. The results of electrochemical studies on MM1 enlarge the known properties of this compound and provide the basis for understanding the electrochemical properties of other tetrahydroacridines. Mixture of solvents could be the solution to see clearly peaks attributed to electroactive compound in the anodic domain, to avoid overlap with the solvent processes. The works are in progress.

Acknowledgement:

The research work was partially supported for materials by National University of Science and Technology Politehnica Bucharest; the authors are thankful to Agence Universitaire de la Francophonie for the support through the grant Petrache Poenaru. Special thanks are directed to the group of organic chemists from our university lead by Matei Raicopol for the fruitful discussions on the electrochemical processes mechanism.

R E F E R E N C E S

[1]. *A. M.-Alonso*. "π-Conjugated Materials: Here. There. and Everywhere". in Chem. Mater.. **vol. 35**. 2023. pp. 1467–1469. https://doi.org/10.1021/acs.chemmater.2c03567.

[2]. *L. Ma. Y. Yu. L. Li. T. Lei. B. Jiao. X. Hou. Z. Wu*. "Efficient amplified spontaneous emission based on π-conjugated fluorophore-cored molecules studied by density functional theory". in Org Electron.. **vol. 57**. 2018. pp. 123–132. https://doi.org/10.1016/j.orgel.2018.02.042; (b) *K. Shizu. H.Noda. H. Tanaka. M. Taneda. M. Uejima. T. Sato. K.i Tanaka. H. Kaji. C. Adachi*. "Highly Efficient Blue Electroluminescence Using Delayed-Fluorescence Emitters with Large Overlap Density between Luminescent and Ground States". in J. Phys. Chem. C .. **vol. 119**. no. 47. 2015. pp. 26283–26289. https://doi.org/10.1021/acs.jpcc.5b07798.

[3]. *T. R. Hong. J. Shin. H. A. Um. T. W. Lee. M. J. Cho. G. W. Kim. J. H. Kwon. D. H. Choi*. "New π-extended diketopyrrolopyrrole-based conjugated molecules for solution-processed solar cells: Influence of effective conjugation length on power conversion efficiency". in Dyes Pigm. **vol. 108**. 2014. pp. 7–14. https://doi.org/10.1016/j.dyepig.2014.04.015.

[4]. *Z.Z. Sun. P.P. Sun. S. Feng. Y.L. Xu. and J.F. Liu*. "Molecular design of D-π-D-typed hole-transporting materials for perovskite solar cells based on the π-conjugated cores". in Synth Met. **vol. 254**. 2019. pp. 34–41. (b) M. *Cigánek. J. Richtár. M. Weiter. J. Krajčovič*. "Organic π-Conjugated Molecules: From Nature to Artificial Applications. Where are the Boundaries?". in Isr. J. Chem.. **vol. 61**. 2021. pp. 1-5. https://doi.org/10.1002/ijch.202100061.

[5]. *R. Kumar. M. Kaur. M. Kumari*. "Acridine: a versatile heterocyclic nucleus". in Acta Pol. Pharm**. vol. 69**. 2012. pp. 3–9; (b*) L.K.M.O. Goni. M.A.J. Mazumder. D.B. Tripathy. M.A. Quraishi*. "Acridine and Its Derivatives: Synthesis. Biological. and Anticorrosion Properties". Materials (Basel).. **vol. 15**. 2022. pp. 7560. doi: 10.3390/ma15217560.

[6]. *M. Demeunynck. F. Charmantray. A. Martelli*. "Interest of acridine derivatives in the anticancer chemotherapy". in Curr. Pharm. Des.. **vol. 7**. 2001. pp. 1703–1724. https://doi.org/10.2174/1381612013397131; *P. Prasher. M. Sharma*. "Medicinal chemistry of acridine and its analogues". in Med. Chem. Comm. **vol. 9**. 2018. pp. 1589–1618. doi: 10.1039/c8md00384j.

[7]. *S. Chatterjee. G.S. Kumar*. "Binding of fluorescent acridine dyes acridine orange and 9-aminoacridine to hemoglobin: Elucidation of their molecular recognition by spectroscopy. calorimetry and molecular modeling techniques". in J. Photochem. Photobiol.. B. **vol. 159**. 2016. pp. 169–178. https://doi.org/10.1016/j.jphotobiol.2016.03.045; (b) *K. Prabakaran. R. Manivannan. H. Oh. C. Parthiban. Y.-A Son*. "Synthesis and characterisation of new acridine dye molecules combined UV absorber and exploring photophysical properties". in Dyes and Pigments. **vol. 192**. 2021. pp. 109391. https://doi.org/10.1016/j.dyepig.2021.109391

[8]. *F. dos Santos Carlos. L. A. da Silva. C. Zanlorenzi. F. Souza Nunes*. "A novel macrocycle acridine-based fluorescent chemosensor for selective detection of Cd2+ in Brazilian sugarcane spirit and tobacco cigarette smoke extract". in Inorganica Chim. Acta.. **vol. 508**. 2020. pp. 119634. https://doi.org/10.1016/j.ica.2020.119634; (b) *P. Ravichandiran. D.S. Prabakaran. N. Maroli. A.R. Kim. B.-H. Park. M.-K. Han. T. Ramesh. S. Ponpandian. D.J. Yoo*. "Mitochondria-targeted acridine-based dual-channel fluorescence chemosensor for detection of Sn^{4+} and $Cr_2O_7^{2-}$ ions in water and its application in discriminative detection of cancer cells". in J. Hazard. Mater.. **vol. 419**. 2021. pp. 126409. https://doi.org/10.1016/j.jhazmat.2021.12640.

[9]. *X. Gong. C. H. Lu. W. K. Lee. P. Li. Y. H. Huang. Z. Chen. L. Zhan. C. C. Wu. S. Gong. C. Yang*. "High-efficiency red thermally activated delayed fluorescence emitters based on benzothiophene-fused spiro-acridine donor". in Chem. Eng. J.. **vol. 405**. 2021. pp. 126663. https://doi.org/10.1016/j.cej.2020.126663; (b) *T. Chen. C.-H. Lu. Z. Chen. X. Gong. C.-C. Wu. C. Yang*. "Modulating the Electron-Donating Ability of Acridine Donor Units for Orange–Red Thermally Activated Delayed Fluorescence Emitters". in Chem. Eur. J.. **vol. 27**. 2021. pp. 3151-3158. https://doi.org/10.1002/chem.202004719.

[10]. *J. Zhang. J. R. Lakowicz*. "Enhanced Luminescence of Phenyl-phenanthridine Dye on Aggregated Small Silver Nanoparticles". in J. Phys. Chem. B.. **vol. 109**. 2005. pp. 8701–8706. https://doi.org/10.1021/jp046016j; (b) *N. Tka. M.A.H Ayed. M.B Braiek. M. Jabli. N. Chaaben.*

K. Alimi. S. Jopp. P. Langer. "2.4-Bis(arylethynyl)-9-chloro-5.6.7.8-tetrahydroacridines: synthesis and photophysical properties". in Beilstein J Org Chem.. **vol. 17**. 2021. pp. 1629-1640. doi: 10.3762/bjoc.17.115.

[11]. *Z. Wang. H. Zhang. Z. Wang. B. Zhao. L. Chen. J. Li. H. Wang. Y. Hao. and W. Li*. "Efficient management of excitons in red and white organic light-emitting diodes by employing blue thermally activated delayed fluorescent emitter based acridine/sulfone derivative as the host". in Org. Electron., **vol. 57**. 2018. pp. 311–316. https://doi.org/10.1016/j.orgel.2018.03.031. .(b) *J. Ding. S. Dong. M. Zhang. F. Li*. "Efficient pure near-infrared organic light-emitting diodes based on tris(2.4.6-trichlorophenyl) methyl radical derivatives". in J. Mater. Chem. C.. **vol. 10**. 2022. pp. 14116-14121. https://doi.org/10.1039/D2TC03299F.

[12]. *W. Zeng. H. Y. Lai. W. K. Lee. M. Jiao. Y. J. Shiu. C. Zhong. S. Gong. T. Zhou. G. Xie. M. Sarma. W. Ken-Tsung. W. Chung-Chih. and Y. Chuluo*. "Achieving Nearly 30% External Quantum Efficiency for Orange–Red Organic Light Emitting Diodes by Employing Thermally Activated Delayed Fluorescence Emitters Composed of 1.8-Naphthalimide-Acridine Hybrids". in Adv. Mater.. **vol. 30**. 2018. pp. 1704961. (b) *N. Tka. M. A. H. Ayed. M. Braiek. M. Jabli. P. Langer*. "Synthesis and investigation on optical and electrochemical properties of 2.4-diaryl-9-chloro-5.6.7.8-tetrahydroacridines". in Beilstein. J. Org. Chem.. **vol. 17**. 2021. pp. 2450–2461. doi: 10.3762/bjoc.17.162.

[13]. *M.C. Pirrung. J.H. Chau. J. Chen*. "Discovery of a novel tetrahydroacridine acetylcholinesterase inhibitor through an indexed combinatorial library." in Chen J. Chem Biol.. **vol. 2**. 1995. pp. 621–626. (b) *P. Olszewska. E. Mikiciuk-Olasik. K. Błaszczak-Świątkiewicz. J. Szymański. P. Szymański*. "Novel tetrahydroacridine derivatives inhibit human lung adenocarcinoma cell growth by inducing G1 phase cell cycle arrest and apoptosis". in Biomed. pharmacother.. **Vol. 68**. 2014. pp. 959-967. https://doi.org/10.1016/j.biopha.2014.10.018.

[14]. *R.G. Gouveia. A.G. Ribeiro. M. Â. S.P. Segundo. J. F. de Oliveira. M. do C. A. de Lima. T. R. C. de L. Souza. S. M. V. de Almeida. R. O. de Moura* "Synthesis. DNA and protein interactions and human topoisomerase inhibition of novel Spiroacridine derivatives". in Bioorg. Med. Chem.. **vol. 26**. 2018. pp. 5911-5921. (b) *C. Martins. M. C. Carreiras. R. León. C. de los Ríos. M. Bartolini. V. Andrisano. I. Iriepa. I. Moraleda. E. Gálvez. M. García. E. Javier. S. Abdelouhaid. C. Mourad. and M-C. José*. "Synthesis and biological assessment of diversely substituted furo[2.3-b] quinolin-4-amine and pyrrolo[2.3-b] quinolin-4-amine derivatives. as novel tacrine analogues". in Eur. J. Med. Chem.. **vol. 46**. 2011. pp. 6119–6130.

[15]. *M. Girek. K. Kłosiński. B. Grobelski. S. Pizzimenti. M. A. Cucci. M. D.. G.Barrera. Z. Pasieka. K. Czarnecka. P. Szymański*. "Novel tetrahydroacridine derivatives with iodobenzoic moieties induce G0/G1 cell cycle arrest and apoptosis in A549 non-small lung cancer and HT-29 colorectal cancer cells". in Mol. Cell. Biochem.. **vol. 460**. 2019. pp. 123–150. doi: 10.1007/s11010-019-03576-x; (b) *S.-L. Wang. Z.-F. Wang. Q.-P. Qin. M.-X. Tan. D.-M. Luo. B.-Q. Zou. Y.-C. Liu*. "A 9 chloro 5.6.7.8 tetrahydroacridine Pt(II) complex induces apoptosis of Hep G2 cells via inhibiting telomerase activity and disrupting mitochondrial pathway. in Inorg. Chem. Commun.. **vol. 99**. 2019. pp. 77–81.

[16]. *G.C. Muscia. G.Y. Buldain. S.E. Asís*. "Design. synthesis and evaluation of acridine and fused-quinoline derivatives as potential anti-tuberculosis agents". in Eur. J. Med. Chem.. **vol. 73**. 2014. pp. 243-249. https://doi.org/10.1016/j.ejmech.2013.12.013G; (b) *R.P. Tripathi. S.S. Verma. J. Pandey. K.C. Agarwal. V. Chaturvedi. Y.K. Manju. A.K. Srivastva. A. Gaikwad. S. Sinha*. "Search of antitubercular activities in tetrahydroacridines: synthesis and biological evaluation". in Bioorg. Med. Chem. Lett.. **vol. 16**. 2006. pp. 5144–5147.

[17]. *M.M. Hrubaru. C.D. Badiceanu. A.C. Ekennia. S.N. Okafor. C. Enache. L. Tarko. V. Tecuceanu. M. Maganu*. "Synthesis. Spectral Characterization and Molecular Docking Studies of Novel Benzidin-bis-tetrahydroacridine Analogues". in Rev. Chim.. **vol. 71**. 2020. pp. 163-181. https://doi.org/10.37358/RC.20.5.8125. (b) *M.M. Hrubaru. M. Maganu. D. Vulpes. M.-G.*

Alexandru. M. Plaveti. "Synthesis and spectral characterization of new methylene-bis-polymethylenquinoline-bis-carboxamides". in Rev. Chim.. **vol. 60**. 2009. pp. 859-862.

[18]. *F.A. Ngounoue Kamga. M.-M. Hrubaru. O. Enache. E. Diacu. C. Draghici. V. Tecuceanu. E.-M. Ungureanu. S. Nkemone. P.T. Ndifon*. "Ni(II)-Salophen—Comprehensive Analysis on Electrochemical and Spectral Characterization and Biological Studies" . in Molecules.. **vol. 28**. 2023. pp. 5464.

[19]. *M.M. Hrubaru. B. Draghici. A. Perescu. F. Badea*. "Synthesis and Spectral Characterisation of Some Substituted Benzamides Deriving from 7-Methoxy-9-Amino-1.2.3.4-Tetrahydroacridines". in Rev. Chim. **vol. 55**. 2004. pp. 773-776.

[20]. *M.M. Hrubaru. A. Stefaniu. N. Murat. M.-R. Bujduveanu. E. Diacu. E.-M. Ungureanu*. "Investigation optique et calculs DFT pour deux tétrahydroacridines". Symposium de la recherche scientifique francophone en Europe centrale et orientale. 27-28 novembre 2023. Bucarest. soumis.

[21]. *J. Rupar. M.M. Aleksić. V. Dobričić. J. Brborić. O. Čudina*. "An electrochemical study of 9-chloroacridine redox behavior and its interaction with double-stranded DNA". In Bioelectrochemistry. **vol. 135**. 2020. pp. 107579. doi:10.1016/j.bioelechem.2020.107

[22]. *D.P. Valencia. F.J. González*. "Estimation of diffusion coefficients by using a linear correlation between the diffusion coefficient and molecular weight". in J. Electroanal. Chem. **Vol. 681**. 2012. pp. 121–126.